

Synthesis and characterization of green-to-yellow emissive Ir(III) complexes of pyridylbenzothiadiazine ligand

Amlan K. Pal, David B. Cordes, Konstantina Pringouri, Muhammad U. Anwar, Alexandra M. Z. Slawin, Jeremy M. Rawson & Eli Zysman-Colman

To cite this article: Amlan K. Pal, David B. Cordes, Konstantina Pringouri, Muhammad U. Anwar, Alexandra M. Z. Slawin, Jeremy M. Rawson & Eli Zysman-Colman (2016) Synthesis and characterization of green-to-yellow emissive Ir(III) complexes of pyridylbenzothiadiazine ligand, Journal of Coordination Chemistry, 69:11-13, 1924-1937, DOI: [10.1080/00958972.2016.1170818](https://doi.org/10.1080/00958972.2016.1170818)

To link to this article: <https://doi.org/10.1080/00958972.2016.1170818>



© 2016 The Author(s). Published by Informa UK Limited, trading as Taylor & Francis Group



Published online: 18 Apr 2016.



Submit your article to this journal [↗](#)



Article views: 1362



View related articles [↗](#)




View Crossmark data [↗](#)



Citing articles: 1 View citing articles [↗](#)

Synthesis and characterization of green-to-yellow emissive Ir(III) complexes of pyridylbenzothiadiazine ligand

Amlan K. Pal^a, David B. Cordes^b , Konstantina Pringouri^c, Muhammad U. Anwar^c,
Alexandra M. Z. Slawin^b, Jeremy M. Rawson^c and Eli Zysman-Colman^a 

^aOrganic Semiconductor Centre, EaStCHEM School of Chemistry, University of St. Andrews, St. Andrews, Fife, UK; ^bEaStCHEM School of Chemistry, University of St. Andrews, St. Andrews, Fife, UK; ^cDepartment of Chemistry and Biochemistry, The University of Windsor, Windsor, Canada

ABSTRACT

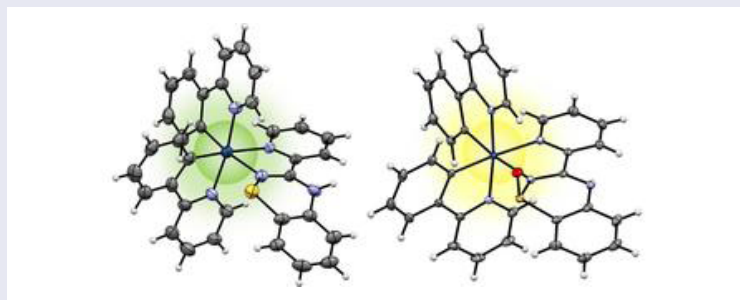
Reaction of tetrakis(2-phenylpyridinato-*C*²,*N'*)(μ -dichloro)di-iridium with 3-(pyridin-2-yl)-4*H*-benzo[e][1,2,4]thiadiazine (**L1**) under neutral and basic media afforded the charged and neutral Ir-complexes, **1** and **2**, respectively, in good yields (63–79%). Single-crystal XRD analysis confirms that the ancillary ligands in both **1** and **2** bind to the iridium via coordination of N₂ of the benzo[e][1,2,4]thiadiazine. Upon isolation of the neutral complex, the sulfur rapidly oxidizes to form **2**. The UV–vis absorption spectra of the complexes exhibit both ligand-centered and mixed metal-to-ligand and ligand-to-ligand charge transfer transitions that are typical of many heteroleptic iridium complexes. Complexes **1** and **2** were emissive at room temperature in the green and yellow region of the electromagnetic spectrum, respectively, albeit with poor photoluminescence quantum yield ($\Phi_{\text{PL}} = 1.1$ –2.5%).

ARTICLE HISTORY

Received 12 January 2016
Accepted 25 February 2016

KEYWORDS

Ir-complex; benzothiadiazine ligand; electrochemistry; photophysics; XRD analysis; DFT studies



1. Introduction

Since the pivotal work by Watts and co-workers [1], interest in the photophysical and electrochemical properties of cationic heteroleptic iridium complexes of the form $[\text{Ir}(\text{ppy})_2(\text{bpy})]^+$, where ppyH is 2-phenylpyridine and bpy is 2,2'-bipyridine, has increased tremendously [2]. Cationic Ir(III) complexes, which have found wide use as emitters in electroluminescent devices [3], as photocatalysts [4] and in biolabeling [5], have been derivatized mostly by incorporation of electron donating or withdrawing

groups onto either the cyclometalating or ancillary ligands [6, 7]. Though several pyridylazole ancillary ligands have been explored as ancillary ligands, the overall structural diversity of heterocycles employed remains relatively poor.

The family of benzo[e][1,2,4]thiadiazine with sulfur in various oxidation states has attracted attention for both materials and pharmaceutical applications [8]. While there are a number of synthetic methodologies to access specific derivatives of fused aryl-1,2,4-thiadiazines depending on the fused substituent [8–10], to the best of our knowledge, until now there is only one report of using 3-(pyridin-2-yl)-4*H*-benzo[e][1,2,4]thiadiazine (**L1**) as a bidentate *N,N'*-chelating ligand, and this with respect to complexation with first row transition metals [11]. We thus became interested to attach **L1** to the [Ir(ppy)₂]⁺ core and study the structure–property relationship of the resulting complexes.

Herein, we report synthesis and characterization of a charged (**1**) and a neutral (**2**) Ir(III) complex, obtained under neutral and basic complexation conditions with **L1**, respectively. The optoelectronic properties of these complexes are discussed in the context of combined experimental and density functional theory (DFT) studies.

2. Experimental

2.1. Chemical and starting materials

All reagents and solvents were of reagent grade and used as supplied. The iridium(III) dimer, tetrakis(2-phenylpyridinato-*C*²,*N'*)(μ -dichloro)diiridium, [Ir(ppy)₂(μ -Cl)]₂ (where ppy=2-phenylpyridinato or 2-phenylpyridine-*C*²,*N'*), was prepared according to the procedure described by Nonoyama [12]. Ligand 3-(pyridin-2-yl)-4*H*-benzo[e][1,2,4]thiadiazine (**L1**) was prepared following the literature procedure [10].

2.2. Instrumentation

2.2.1. For purification, NMR spectroscopy, melting point determination and mass spectrometry

All reactions were performed using standard Schlenk techniques under an inert (N₂) atmosphere with reagent grade solvents. Flash column chromatography was performed using silica gel (Silia-P from Silicycle, 60 Å, 40–63 mm). Analytical thin layer chromatography was performed with silica plates with aluminum backings (250 mm with indicator F-254). Compounds were visualized under UV light. ¹H and ¹³C NMR spectra were recorded on a Bruker Avance spectrometer at 500 and 126 MHz, respectively. Deuterated chloroform (CDCl₃) and deuterated acetonitrile (CD₃CN) were used as solvents of record and TMS was used as an internal standard. Melting points (Mps) were recorded using open-ended capillaries on an electrothermal melting point apparatus and are uncorrected. For high-resolution mass spectrometry the compounds were dissolved in DCM before being diluted in MeOH with NH₄OAc for analysis on the Thermo Scientific LTQ Orbitrap XL in positive nano-electrospray ionization mode. The instrument was calibrated with a mixture of caffeine, UltraMark and MRFA.

2.2.2. For cyclic voltammetry

Electrochemical measurements were carried out in N₂-purged purified MeCN at 25 °C with a Potentiostat CH620E instrument. The working electrode was glassy carbon, the counter electrode was a Pt wire, and the pseudo-reference electrode was a Ag wire. The reference was an internal 1 mM solution of ferrocene/ferrocinium (380 mV *versus* SCE in MeCN) [13]. The concentration of the compounds analyzed was 1 mM. Tetra-*n*-butylammonium hexafluorophosphate was used as the supporting electrolyte (0.10 M). Cyclic voltammograms of **1** and **2** were obtained at a scan rate of 100 mV s⁻¹. The criteria for reversibility were (a) a separation of 60 mV between cathodic and anodic peaks, (b) a ratio of the intensities of the cathodic and anodic currents > 0.9, and (c) the lack of dependency of the peak potential on scan rate.

2.2.3. For UV-vis absorption spectroscopy

Electronic spectra were recorded using a Shimadzu UV-1800 double beam spectrophotometer with a 1 cm quartz cell from 200–1000 nm at room temperature. All samples were prepared in HPLC grade acetonitrile with varying concentrations in the order of mM. Molar absorptivity determination was verified by linear least-squares fit of values obtained from at least four independent solutions at varying concentrations with absorbance ranging from 8.08×10^{-5} to 8.99×10^{-6} M. Broad peaks are marked as shoulder, "sh".

2.2.4. For steady-state and time-resolved emission spectroscopy

Steady-state emission and excitation spectra and time-resolved emission spectra were recorded at 298 K using an Edinburgh Instruments F980. The sample solutions for the emission spectra were prepared in HPLC-grade acetonitrile and degassed via three freeze-pump-thaw cycles. Luminescence lifetimes were determined by time-correlated single-photon counting with an Edinburgh EPL-378 spectrometer (nanosecond-pulse diode laser at 378 nm). All samples for steady-state measurements were excited at 360 nm while samples for time-resolved measurements were excited at 378 nm.

2.2.5. For determination of photoluminescence quantum yield

Photoluminescence quantum yields (Φ_{PL}) were determined using the optically dilute method [14, 15]. A stock solution with absorbance of ca. 0.5 was prepared and then four dilutions were prepared with dilution factors of 5, 6.6, 10, and 20 to obtain solutions with absorbances of ca. 0.1, 0.075, 0.05 and 0.025, respectively. The Beer-Lambert law was found to be linear at the concentrations of the solutions. The emission spectra were then measured after the solutions were rigorously degassed via three freeze-pump-thaw cycles prior to spectrum acquisition. For each sample, linearity between absorption and emission intensity was verified through linear regression analysis and additional measurements were acquired until the Pearson regression factor (R^2) for the linear fit of the data-set surpassed 0.9. Individual relative quantum yield values were calculated for each solution and the values reported represent the slope value. The equation $\Phi_s = \Phi_r (A_r/A_s)(I_s/I_r)(n_s/n_r)^2$ was used to calculate the relative quantum yield of each of the samples, where Φ_r is the absolute quantum yield of the reference, n is the refractive index of the solvent, A is the absorbance at the excitation wavelength, and I is the integrated area under the corrected emission curve. The subscripts s and r refer to the sample and reference, respectively. A solution of quinine sulfate in 0.5 M H_2SO_4 ($\Phi_r = 54.6\%$) was used as the external reference [16].

2.3. X-ray crystallography

X-ray diffraction data for **1** and **2** were collected at 173 K using a Rigaku FR-X Ultrahigh brilliance Microfocus RA generator/confocal optics and Rigaku XtaLAB P200 system, with Mo K α radiation ($\lambda = 0.71075 \text{ \AA}$). Intensity data were collected using ω steps accumulating area detector images spanning at least a hemisphere of reciprocal space. All data were corrected for Lorentz polarization effects. A multiscan absorption correction was applied by using CrystalClear [17]. Structures were solved by Patterson (PATTY [18]) methods and refined by full-matrix least-squares against F^2 (SHELXL-2013 [19]). Non-hydrogen atoms were refined anisotropically and hydrogens were refined using a riding model. All calculations were performed using the CrystalStructure [20] interface. Crystallographic data are summarized in table 1.

2.4. Syntheses of complexes

2.4.1. Synthesis of bis(2-phenylpyridinato- C^2, N')(3-(pyridin-2-yl)-4H-benzo[e][1,2,4]thiadiazine) iridium(III) hexafluorophosphate, **1**

A 100 mL round-bottomed flask was charged with $[\text{Ir}(\text{ppy})_2(\mu\text{-Cl})_2]$ (0.100 g, 0.093 mmol, 1 equiv.) and 3-(pyridin-2-yl)-4H-benzo[e][1,2,4]thiadiazine (0.041 g, 0.193 mmol, 2.07 equiv.), **L1**. An aliquot of a mixture of dichloromethane and methanol (40 mL, 1 : 1, v/v) was added to the flask and the solution

Table 1. Crystallographic data for **1** and **2**.

Compound	1	2
CCDC	1445661	1445662
Formula	[C ₃₄ H ₂₅ N ₅ SiIr][PF ₆]	[C ₃₄ H ₂₄ N ₅ OSiIr]·CH ₂ Cl ₂
<i>M</i> w (g mol ⁻¹)	872.82	827.77
<i>d</i> _{calc} (g cm ⁻³)	1.830	1.782
<i>F</i> (0 0 0)	1704	1624
Crystal system	Monoclinic	Monoclinic
Space group	<i>P</i> ₂ <i>1</i> / <i>n</i>	<i>P</i> ₂ <i>1</i> / <i>c</i>
<i>a</i> (Å)	9.6076(14)	18.0512(12)
<i>b</i> (Å)	14.0382(19)	9.4690(6)
<i>c</i> (Å)	23.582(4)	19.5919(15)
β (°)	95.079(4)	112.8760(17)
<i>V</i> (Å ³)	3168.1(8)	3085.4(4)
<i>Z</i>	4	4
θ range (°)	1.69–25.388	2.108–25.376
Completeness	0.990	0.996
Reflections collected	26786	36797
Independent reflections (<i>R</i> _{int})	3558 (0.1127)	5325 (0.0208)
μ (mm ⁻¹)	4.401	4.607
<i>R</i> 1 ^a	0.0657	0.0140
<i>wR</i> 2 ^a	0.1730	0.0358
GoF ^a	1.077	1.056
Residual electron density: max., min.	2.328, -0.806	0.845, -0.641

^a*R*1 based on observed reflections with *I* > 2 σ (*I*) for **1**, and **2**; *wR*2 and GoF based on all data for all compounds.

was degassed with nitrogen. The solution was heated to reflux under nitrogen, for 20 h, after which the solution was cooled to room temperature and the solvent was evaporated to dryness under reduced pressure to afford a red solid. Purification by flash column chromatography (silica, dichloromethane/methanol, 97:3, v/v) and subsequent anion metathesis by addition of an aliquot of saturated solution of KPF₆ in water afforded **1** as a red solid. Crystals of suitable X-ray quality were grown by slow diffusion of diethyl ether into a concentrated solution of **1** in dichloromethane. Yield: 0.131 g, 79%. *R*_f: 0.45 (dichloromethane/methanol, 97:3, v/v on silica). M.p.: 328–330 °C (dec.). ¹H NMR (500 MHz, CD₃CN) δ (ppm): 6.18 (dt, *J* = 7.69, 1.28 Hz, 2 H), 6.47 (d, *J* = 7.69 Hz, 1 H), 6.81–6.89 (m, 3 H), 6.94 (td, *J* = 7.69, 1.28 Hz, 1 H), 6.97–7.08 (m, 3 H), 7.17 (ddd, *J* = 7.43, 5.82, 1.50 Hz, 1 H), 7.30 (ddd, *J* = 7.43, 5.82, 1.50 Hz, 1 H), 7.51–7.57 (m, 2 H), 7.76 (ddd, *J* = 7.75, 3.15, 1.28 Hz, 2 H), 7.86–7.92 (m, 2 H), 7.95 (td, *J* = 7.85, 1.60 Hz, 1 H), 8.03 (d, *J* = 7.91 Hz, 1 H), 8.10 (d, *J* = 7.91 Hz, 1 H), 8.13–8.18 (m, 2 H), 8.48 (s, 1 H), 8.67–8.72 (m, 1 H). ¹³C NMR (126 MHz, CD₃CN) δ (ppm): 167.75, 167.09, 161.05, 150.59, 150.23, 149.58, 149.37, 149.04, 148.02, 144.53, 144.16, 138.78, 138.57, 138.45, 137.38, 135.01, 132.07, 131.34, 130.22, 129.76, 129.34, 128.61, 126.74, 126.32, 124.79, 124.43, 123.82, 123.55, 122.50, 122.42, 122.37, 119.66, 119.35, 118.37. HR NSI⁺ MS: [M + O–PF₆]⁺ Calculated: 744.1409 (C₃₅H₂₅N₅OSiIr); Found: 744.1388. Anal. Calcd for C₃₄H₂₅N₅SiIrPF₆ (%): C, 46.79; H, 2.89; N, 8.02. Found: C, 47.30; H, 3.01; N, 7.80.

2.4.2. Synthesis of bis(2-phenylpyridinato-C²,N')(3-(pyridin-2-yl)-2 λ^2 -benzo[e][1,2,4]thiadiazine-1-oxide)iridium(III), **2**

A 100 mL round-bottomed flask was charged with 3-(pyridin-2-yl)-4H-benzo[e][1,2,4]thiadiazine, **L1** (0.041 g, 0.193 mmol, 2.07 equiv. with respect to Ir-dimer), and anhydrous K₂CO₃ (0.270 g, 1.93 mmol, 10 equiv. with respect to **L1**). Methanol (30 mL) was added to the flask and the solution was degassed with nitrogen. The solution was heated to reflux under nitrogen for 30 min, after which the clear yellow solution was cooled to room temperature. To this solution was added a solution of [Ir(ppy)₂(μ -Cl)]₂ (0.100 g, 0.093 mmol, 1 equiv.) in dichloromethane (20 mL), and an immediate color change to dark brown was observed. The mixture of solutions was degassed with N₂ and then heated to reflux for 20 h under N₂. After 20 h, the solution was cooled to room temperature, then filtered through a fine glass frit. The residue was washed with MeOH (5 mL) and the filtrate and washings were combined and evaporated to dryness under reduced pressure to afford a brownish-yellow solid. Purification of

this product by flash column chromatography (30 cm long) (silica, 0.5–1% MeOH in DCM) afforded the S-oxidized S(IV) **2** as a yellow solid. Crystals of suitable X-ray quality were grown by slow diffusion of diethyl ether into a concentrated solution of **2** in dichloromethane. Yield: 0.086 g, 63%. R_f : 0.52 (1% MeOH in DCM on silica). M.p.: 368–372 °C (dec.). $^1\text{H NMR}$ (500 MHz, CD_3CN) δ (ppm): 6.25 (d, $J = 7.69$ Hz, 1 H), 6.46 (d, $J = 7.48$ Hz, 1 H), 6.83 (td, $J = 7.32, 4.17$ Hz, 2 H), 6.92–7.00 (m, 3 H), 7.10 (t, $J = 6.62$ Hz, 1 H), 7.20 (t, $J = 7.37$ Hz, 1 H), 7.24 (d, $J = 7.27$ Hz, 1 H), 7.34 (t, $J = 6.52$ Hz, 1 H), 7.40–7.44 (m, 1 H), 7.47–7.52 (m, 1 H), 7.67 (d, $J = 5.56$ Hz, 1 H), 7.70–7.82 (m, 5 H), 7.96–8.03 (m, 3 H), 8.73 (d, $J = 7.91$ Hz, 1 H), 9.40 (d, $J = 5.98$ Hz, 1 H). $^1\text{H NMR}$ (500 MHz, CDCl_3) δ (ppm): 6.28 (dd, $J = 7.48, 0.85$ Hz, 1 H), 6.62 (dd, $J = 7.48, 0.85$ Hz, 1 H), 6.78–6.84 (m, 2 H), 6.90 (td, $J = 7.43, 1.39$ Hz, 1 H), 6.97 (tdd, $J = 7.51, 7.51, 2.51, 1.28$ Hz, 2 H), 7.05–7.09 (m, 1 H), 7.15–7.22 (m, 2 H), 7.38 (dt, $J = 7.59, 1.02$ Hz, 1 H), 7.43–7.46 (m, 2 H), 7.52–7.56 (m, 1 H), 7.58–7.70 (m, 4 H), 7.72–7.75 (m, 1 H), 7.81–7.88 (m, 3 H), 8.79–8.83 (m, 1 H), 9.61 (dd, $J = 5.98, 0.85$ Hz, 1 H). $^{13}\text{C NMR}$ (126 MHz, CDCl_3) δ (ppm): 168.78, 167.63, 159.43, 156.41, 153.13, 153.00, 150.80, 148.69, 148.44, 144.95, 1143.57, 140.43, 137.02, 136.99, 136.85, 133.19, 132.04, 131.06, 130.42, 130.06, 127.33, 127.10, 126.88, 126.75, 125.58, 125.45, 124.32, 124.11, 122.98, 122.19, 121.72, 121.48, 119.06, 118.34. HR NSI⁺ MS: $[\text{M} + \text{H}]^+$ Calculated: 744.1409 ($\text{C}_{34}\text{H}_{25}\text{N}_5\text{OSIr}$); Found: 744.1405. Anal. Calcd for $\text{C}_{34}\text{H}_{24}\text{N}_5\text{OSIr}\cdot\text{CH}_2\text{Cl}_2$ (%): C, 50.78; H, 3.17; N, 8.46. Found: C, 50.75; H, 3.08; N, 8.57.

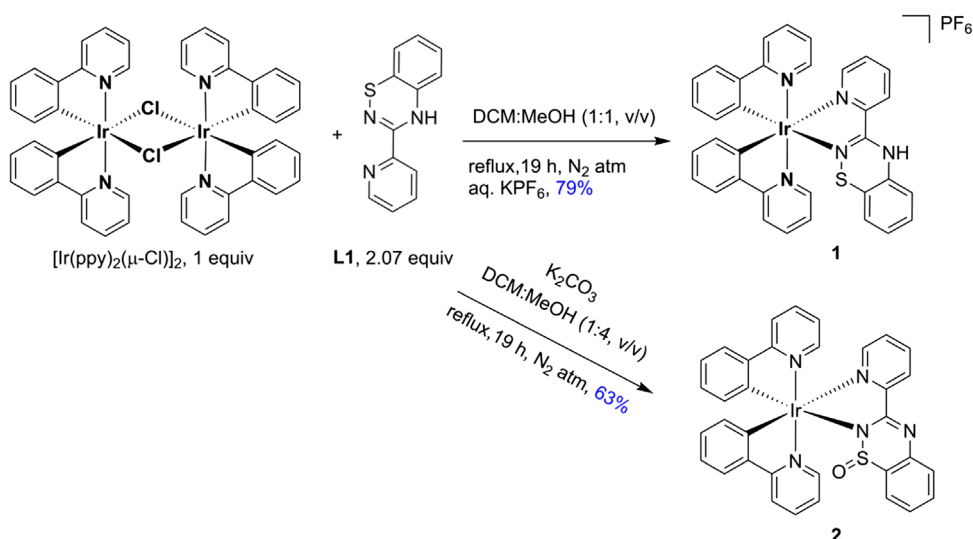
2.5. DFT studies

All calculations were performed with the Gaussian 03 [21] suite of programs employing the DFT method, the Becke three-parameter hybrid functional [22] and Lee-Yang-Parr's gradient-corrected correlation functional (B3LYP) [23]. Singlet ground-state geometry optimizations for $[\mathbf{1}]^+$ (**1** without associated anion) and neutral **2** were carried out at the (R)B3LYP level in the gas phase, using the structures of **1** and **2** determined by X-ray crystallography as starting points. All elements except Ir were assigned the 6–31G(d,p) basis set [24]. The double- ζ quality LANL2DZ ECP basis set [25] with an effective core potential and one additional f-type polarization functional was employed for Ir. Vertical electronic excitations based on (R)B3LYP-optimized geometries were computed for $[\mathbf{1}]^+$, **2** and a model complex, $[\text{Ir}(\text{ppy})_2(\text{bpy})]^+$ using the TD-DFT formalism [26, 27] in MeCN using the conductor-like polarizable continuum model [28–30]. Vibrational frequency calculations were performed to ensure that the optimized geometries represent the local minima, and there are only positive eigenvalues. The electronic distribution and localization of the singlet excited states were visualized using the electron density difference maps. *GaussSum* 2.2 [31] and *Chemissian* [32] were employed to visualize the absorption spectra (simulated with Gaussian distribution with a full-width at half maximum (fwhm) set to 3000 cm^{-1}) and to calculate the fractional contributions of various groups to each molecular orbital. All calculated structures and Kohn-Sham orbitals were visualized with *ChemCraft* [33].

3. Results and discussion

3.1. Synthesis and characterization of the complexes

The Ir(III)-complexes **1** and **2** were synthesized involving a protocol that proceeds via isolation of the μ -dichloro-bridged Ir(III)-dimer described by Nonoyama¹² followed by its cleavage with 2.1 equiv. of ancillary **L1** (scheme 1). The charged **1** was synthesized by reaction of $[\text{Ir}(\text{ppy})_2\text{Cl}]_2$ with **L1** in a N_2 -degassed dichloromethane-methanol solution, whereas the synthesis of the neutral **2** requires *a priori* deprotonation of **L1** with 10 equiv. of anhydrous K_2CO_3 in N_2 -degassed methanol followed by its addition to a N_2 -degassed dichloromethane solution of the Ir-dimer. Despite maintaining the N_2 -atmosphere, the neutral complex was isolated as the S(IV) complex, **2**. The facile oxidation of ligand **L1** is indicative of the electron-rich benzothiadiazinate heterocycle, which has been previously observed by Rawson *et al.*, where **L1** undergoes facile Cu(II)-promoted aerial oxidation to give access to the benzothiadiazine-S-oxide heterocycle [34].



Scheme 1. Syntheses of charged and neutral Ir(III)-complexes, **1** and **2**, respectively, using 3-(pyridin-2-yl)-4*H*-benzo[*e*][1,2,4]thiadiazine, **L1**, as an ancillary ligand.

Complexes **1** and **2** were characterized by ^1H and ^{13}C NMR spectroscopy, melting point determination, HR ESI-MS, elemental analysis and single-crystal XRD analysis. Incorporation of **L1** onto the iridium renders an unsymmetrical coordination environment of the $[\text{Ir}(\text{ppy})_2]$ -moiety as demonstrated by the stacked ^1H NMR spectra of **1** and **2** (figure 1). The HR ESI-MS spectra show the molecular ion for **1**, where the S-atom is oxidized under the mass spectrometric conditions as $[\text{M} + \text{O-PF}_6]^+$, and a protonated analog for **2**, $[\text{M} + \text{H}]^+$.

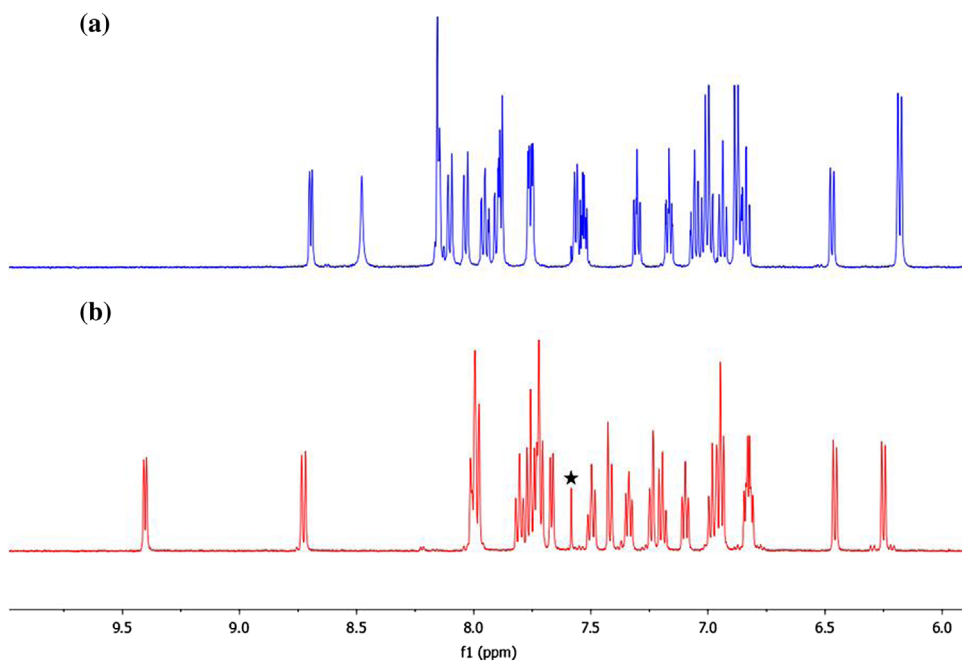


Figure 1. Stacked ^1H NMR spectra of (a) **1** and (b) **2** at room temperature in CD_3CN at 500 MHz (the singlet peak, marked with a star at 7.58 ppm in the spectrum of **2**, is due to contamination of CHCl_3 in CD_3CN).

Table 2. Comparison of observed bond distances and angles in **1** and **2** with values calculated for **1** and **2**.

Compound	Bond lengths (Å)		Angles (°)			
	Obs. (X-ray)	Calcd (DFT)		Obs. (X-ray)	Calcd (DFT)	
1	Ir1–N1	2.058(9)	2.08508	N1–Ir1–C8	80.7(4)	80.057
	Ir1–N13	2.051(9)	2.08354	N13–Ir1–C20	80.0(5)	80.053
	Ir1–N25	2.139(9)	2.23065	N25–Ir1–N32	74.9(3)	73.414
	Ir1–N32	2.148(9)	2.21953	N32–C31–N40	124.9(10)	123.725
	Ir1–C8	2.016(10)	2.01846			
	Ir1–C20	2.005(12)	2.02118			
	C31–N32	1.288(14)	1.30269			
	C31–N40	1.355(14)	1.37633			
	N32–S33	1.715(9)	1.73725			
	2	Ir1–N1	2.0573(17)	2.08768	N1–Ir1–C8	80.10(8)
Ir1–N13		2.0390(17)	2.07360	N13–Ir1–C20	80.02(8)	80.046
Ir1–N25		2.1424(17)	2.21791	N25–Ir1–N32	75.61(7)	74.874
Ir1–N32		2.1650(17)	2.20919	N32–C31–N40	130.21(19)	129.994
Ir1–C8		2.017(2)	2.02430			
Ir1–C20		2.013(2)	2.01864			
C31–N32		1.359(3)	1.35920			
C31–N40		1.314(3)	1.31238			
N32–S33		1.6693(18)	1.71308			

3.2. Solid-state structures

Crystals suitable for analysis by X-ray diffraction were grown by slow vapor diffusion of diisopropyl ether into an acetonitrile solution of **1**, or of diethyl ether into a solution of **2** in dichloromethane (CCDC 1445661 and 1445662). Specific crystallographic parameters in comparison to those obtained from DFT calculations are summarized in table 2. Both structures reveal coordinatively saturated Ir(III) in a distorted octahedral geometry, where in both complexes **L1** binds to Ir(III) in an *N,N'*-chelate fashion (figure 2). The Ir–N_{ppy} and Ir–C_{ppy} bond lengths and C_{ppy}–Ir–N_{ppy} and N_{L1}–Ir–N_{L1} bite angles were similar in both complexes and fall in close agreement with those calculated by DFT. Noticeable differences in bond lengths and angles are observed in the N32–C31–N40 fragments of the neutral and anionic versions of **L1** in **1** and **2**, respectively. In **1**, the shorter C31–N32 bond length compared to that of C31–N40 indicates localized double- and single-bond characters for C31–N32 and C31–N40, respectively. In **2**, due to the anionic nature of **L1**, there is a delocalized double bond character throughout the N32–C31–N40 core. Similarly, there is a more defined sp² character to C31 of the N32 = C31–N40 core in **1** compared to relatively less defined sp² character of the same core in **2**, as judged by the deviation of N32–C31–N40 angle from the ideal sp² bond angle of 120°. The decrease in N32–S33 bond length in **2** compared to that in **1** is presumably due to extended delocalization of the N40–C31–N32–S33–O33 moiety in **2**.

3.3. UV–vis absorption properties of **1** and **2**

The UV–visible absorption spectra of **L1**, **1** and **2** were recorded in MeCN solutions at room temperature (figure 3) and data are summarized in table 3. Overlays of experimental absorption spectra of **1** and **2** with their predicted singlet transitions calculated by time-dependent DFT (TD-DFT) are shown in figure 4. At higher energy (≤ 290 nm), ligand-centered (LC) $\pi \rightarrow \pi^*$ transitions are observed for both complexes. In the case of **1**, the transitions at 374 and 413 nm are predominantly due to singlet ligand-to-ligand charge transfer (¹LLCT), transitions, originating from ppy-to-**L1** with a minor contribution of singlet metal-to-ligand charge transfer (¹MLCT) transition involving Ir(*d* π) \rightarrow **L1**(π^*), as predicted by TD-DFT (table 4). In the case of **2**, the contribution from the metal center comes into play at much higher energies as in the transition at 292 nm (table 5). The transitions at 368, 390 and 444 nm are all composed of a predominant ¹LLCT character along with a minor component of ¹MLCT transition. The tailing of the lowest energy ¹CT transition of **1** at 413 nm up to ~ 560 nm compared to that of **2** ($\lambda_{\text{max}} = 444$ nm) and that of the prototype [Ir(ppy)₂(bpy)]⁺ ($\lambda_{\text{max}} = 465$ nm) is in agreement with the trends revealed from the

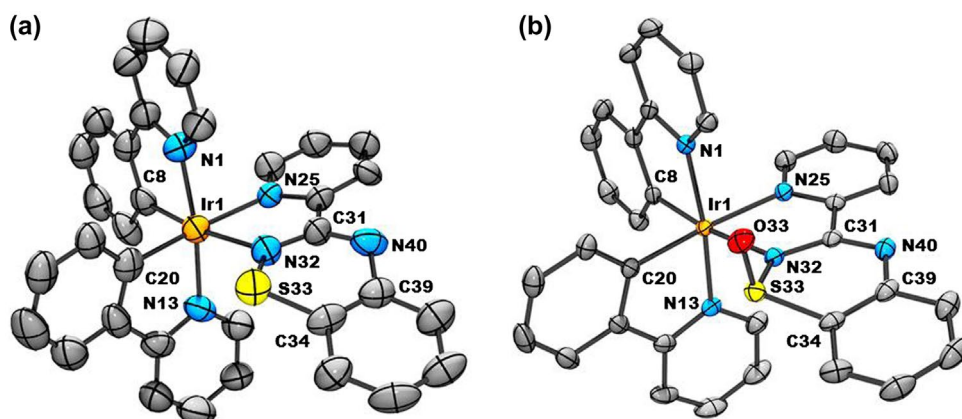


Figure 2. Thermal ellipsoid plots of (a) **1** and (b) **2**. Thermal ellipsoids are drawn at a 50% probability level. Hydrogens, PF_6^- and dichloromethane molecules have been omitted for clarity.

DFT-calculated HOMO–LUMO energy gaps: **1** ($|\Delta E^1_{\text{LUMO-HOMO}}| = 3.06 \text{ eV}$); **2** ($|\Delta E^2_{\text{LUMO-HOMO}}| = 3.47 \text{ eV}$); $[\text{Ir}(\text{ppy})_2(\text{bpy})]^+$ ($|\Delta E_{\text{LUMO-HOMO}}| = 3.22 \text{ eV}$) (figure 5).

3.4. Electrochemical properties of **1** and **2**

The redox behaviors of **L1**, **1** and **2** in dry degassed MeCN were assessed by cyclic voltammetry at room temperature (table 6). **L1** exhibited two quasi-reversible oxidations at 0.66 and 0.95 V, whereas two irreversible reductions were also observed at sufficiently high negative potentials ($> -1.80 \text{ V}$). The relatively easy oxidation of **L1** is indicative of its electron richness and is associated with a proton-coupled 1e-oxidation to form the benzothiadiazinyl radical. At positive potentials, **1** exhibited two irreversible

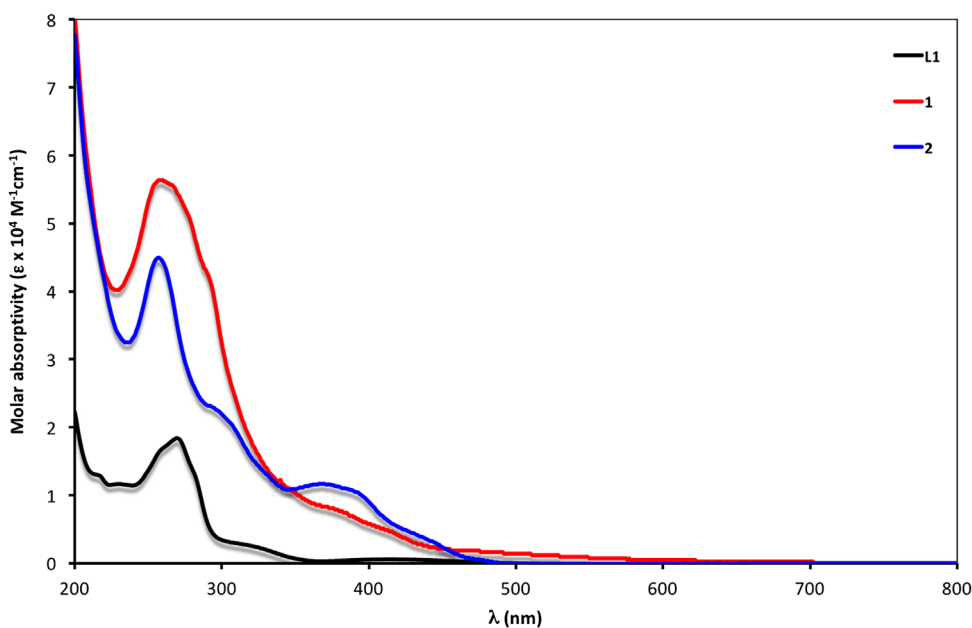
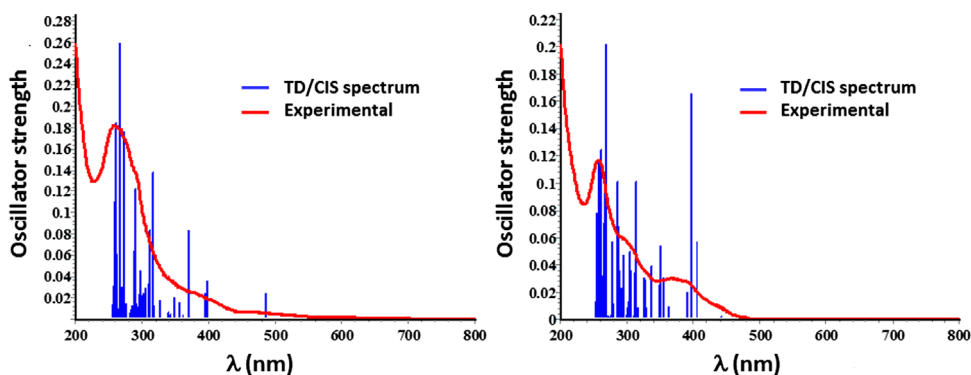


Figure 3. UV–vis absorption spectra of **L1**, **1** and **2** at room temperature in acetonitrile.

Table 3. Absorption data of **L1**, **1**, and **2** and the benchmark complex $[\text{Ir}(\text{ppy})_2(\text{bpy})]\text{PF}_6$ in acetonitrile at room temperature.

Compound	λ_{abs} (nm) ($\epsilon \times 10^3 \text{ M}^{-1} \text{ cm}^{-1}$)
L1	215 (13.0), 231 (11.6), 270 (18.5), 318 (2.7), 412 (6.2)
1	258 (56.8), 292 sh (41.8), 374 sh (7.8), 413 sh (4.2)
2	256 (43.3), 292 (22.7), 368 (11.5), 390 sh (10.5), 444 sh (3.1)
$[\text{Ir}(\text{ppy})_2(\text{bpy})]\text{PF}_6^a$	255 (45.2), 265 sh (43.5), 274 sh (37.4), 311 sh (19.4), 337 sh (8.6), 376 sh (5.6), 411 sh (3.3), 465 sh (0.67)

^aFrom Ref. [35].**Figure 4.** Overlay of experimental UV-vis absorption spectra of **1** (left) and **2** (right) with their predicted transitions calculated by singlet TD-DFT at room temperature in acetonitrile.**Table 4.** Selected transitions from TD-DFT calculations of $[\mathbf{1}]^+$ in the singlet ground state (B3LYP/LANL2DZ(f)[Ir]6-31G**[C,H,N,S], CPCM (MeCN)).

State	λ_{abs} (nm) (TD-DFT)	λ_{abs} (nm) ($\epsilon \times 10^3 \text{ M}^{-1} \text{ cm}^{-1}$) [expt.]	f (TD-DFT)	Major transition(s)	Character
45	261	258 (56.8)	0.1841	H-8 \rightarrow L (10%), H-4 \rightarrow L + 4 (15%), H-2 \rightarrow L + 5 (10%), H \rightarrow L + 8 (13%)	ppy(π) to ppy(π^*) + ppy(π) to L1(π^*) + L1(π) to L1(π^*)
29	290	292 (41.8)	0.1223	H-5 \rightarrow L + 1 (43%), H-3 \rightarrow L + 1 (10%), H-3 \rightarrow L + 3 (14%)	ppy(π) to ppy(π^*) + ppy(π) to L1(π^*)
7	370	374 (7.8)	0.0832	H-4 \rightarrow L (71%)	ppy(π) to L1(π^*) (Major) + Ir($d\pi$) to L1(π^*) (minor)
4	398	413 (4.2)	0.0358	H-3 \rightarrow L (30%), H \rightarrow L + 1 (55%)	ppy(π) to ppy(π^*) and L1(π^*) (Major) + Ir($d\pi$) to L1(π^*) and ppy(π^*) (minor)
1	527	–	0.0008	H \rightarrow L (98%)	ppy(π) to L1(π^*) (Major) + Ir($d\pi$) to L1(π^*) (minor)

oxidations at 1.04 and 1.32 V. The first oxidation wave is assigned to oxidation of an admixture of both metal- and ligand-based orbitals as the HOMO is constituted with almost equal metal and ppy based orbitals (figure 5). This oxidation is significantly cathodically shifted compared to that of $[\text{Ir}(\text{ppy})_2(\text{bpy})]\text{PF}_6$ where $E_{\text{ox}} = 1.27 \text{ V}$ [36]. At negative potentials, two irreversible reductions at -1.19 and -1.64 V and a quasi-reversible reduction at -1.99 V are observed, the first of which is assigned to **L1**-based reduction as inferred by DFT calculations. The second and third reductions are localized almost exclusively on the ppy ligands. The last reduction at -1.99 V , which is associated with ppy, has a peak separation of 30 mV and is thus linked to a two-electron process. The irreversible reduction of **L1** is in contrast to the reversible

Table 5. Selected transitions from TD-DFT calculations of **[2]** in the singlet ground state (B3LYP/LANL2DZ(f)[Ir]6–31G**[C,H,N,O,S], CPCM (MeCN)).^a

State	λ_{abs} (nm) (TD-DFT)	λ_{abs} (nm) ($\epsilon \times 10^3 \text{ M}^{-1} \text{ cm}^{-1}$) [expt.]	f (TD-DFT)	Major transition(s)	Character
44	261	256 (43.3)	0.1248	H-4 \rightarrow L + 4 (22%), H-2 \rightarrow L + 5 (13%), H \rightarrow L + 7 (21%), H \rightarrow L + 8 (18%)	ppy(π) to ppy(π^*) + ppy(π) to aL1(π^*) + aL1(π) to aL1(π^*)
29	286	292 (22.7)	0.1011	H-5 \rightarrow L + 1 (23%), H-3 \rightarrow L + 3 (33%)	ppy(π) to ppy(π^*) (major) + Ir($d\pi$) to aL1(π^*) (minor)
6	356	368 (11.5)	0.0304	H-1 \rightarrow L + 2 (81%)	aL1(π) to ppy(π^*) (Major) + Ir($d\pi$) to ppy(π^*) (minor)
3	397	390 (10.5)	0.1662	H-1 \rightarrow L (79%), H \rightarrow L + 2 (10%)	aL1(π) to aL1(π^*) (Major) + Ir($d\pi$) to aL1(π^*) (minor)
1	441	444 (3.1)	0.0023	H \rightarrow L (98%)	ppy(π) to aL1(π^*) (Major) + Ir($d\pi$) to aL1(π^*) (minor)

^aAnionic form of L1 is abbreviated as aL1 (where aL1 = 3-(pyridin-2-yl)benzo[e][1,2,4]thiadiazin-2-ide-1-oxide).

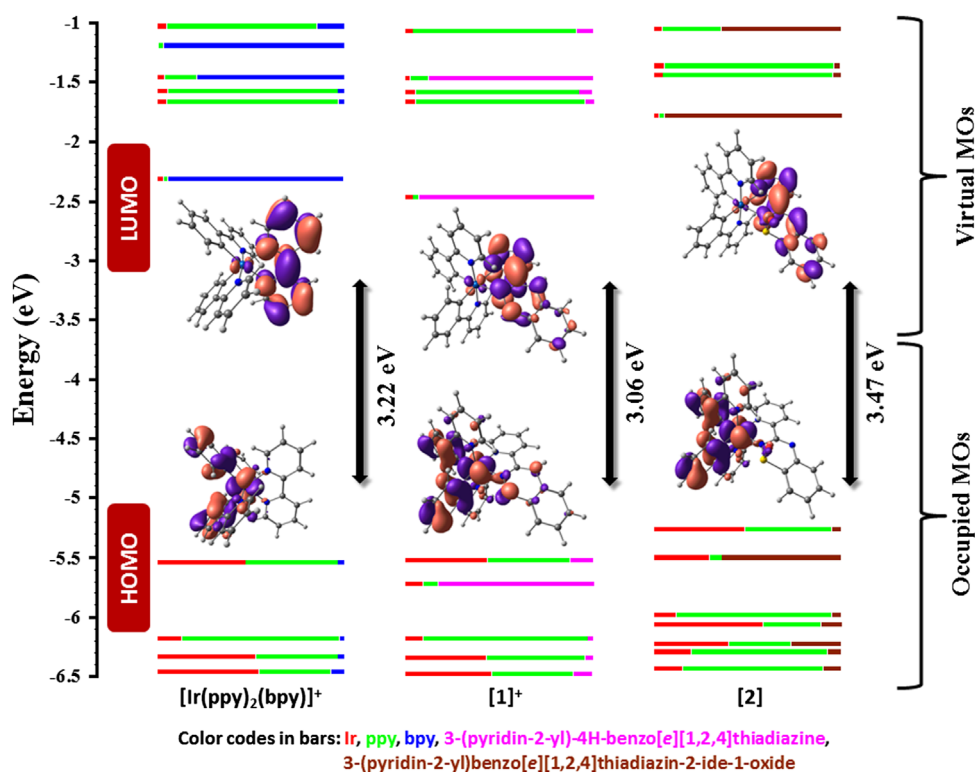


Figure 5. Calculated frontier MO energies of **[1]⁺**, **2** and **[Ir(ppy)₂(bpy)]⁺**, obtained from TD-DFT [(B3LYP/LANL2DZ(f) for Ir(III)) and (6–31 g** for C,H,N,(O),S)] with CPCM(CH₃CN) and 0.5 eV threshold of degeneracy. Kohn-Sham MOs of **[1]⁺**, **2** and **[Ir(ppy)₂(bpy)]⁺** are also shown.

reduction of bpy observed for **[Ir(ppy)₂(bpy)]PF₆** [36], and points to a first reduction in **1** localized on the benzothiadiazine. Complex **2** displayed a (metal + ppy)-based irreversible oxidation at 1.03 V in the anodic region followed by a monoelectronic quasi-reversible oxidation at 1.23 V. Three monoelectronic

Table 6. Electrochemical data^a of **L1**, **1**, **2**, and [Ir(ppy)₂(bpy)]PF₆^c.

Compound	$E_{1/2}^{1, \text{ox}}/V(\Delta E_p)$	$E_{\text{pa}}^{2, \text{ox}}/V(\Delta E_p)$	$E_{1/2}^{1, \text{red}}/V(\Delta E_p)$	$E_{\text{pc}}^{2, \text{red}}/V(\Delta E_p)$	$E_{\text{pc}}^{3, \text{red}}/V(\Delta E_p)$	$E_{\text{pc}}^{4, \text{red}}/V(\Delta E_p)$	$\Delta E/N$	$E_{\text{HOMO}}^{\text{eV}}/V(\Delta E_p)$	$E_{\text{LUMO}}^{\text{eV}}/V(\Delta E_p)$	$ E_{\text{LUMO}}^{\text{eV}} - E_{\text{HOMO}}^{\text{eV}} /V(\Delta E_p)$
L1	0.66 (130)	0.95 (110)	-1.90 (irr) ^b	-2.43 (irr) ^b	—	—	2.56	—	—	—
1	1.04 (irr) ^b	1.32 (irr) ^b	-1.19 (irr) ^b	-1.64 (irr) ^b	-1.99 (30)	—	2.23	-5.53	-2.47	3.06
2	1.03 (irr) ^b	1.23 (94)	-1.83 (69)	-2.11 (ads) ^c	-2.32 (60)	-2.47 (113)	2.86	-5.26	-1.79	3.47
[Ir(ppy) ₂ (bpy)] PF ₆ ^d	1.27 (56)	—	-1.38 (55)	—	—	—	2.65	-5.54	-2.32	3.22

^aPotentials are in volts vs. SCE for MeCN solutions (0.1 M in Bu₄NPF₆) recorded at room temperature. The difference between cathodic and anodic peak potentials, ΔE_p (millivolts) is given in parentheses.

^bIrreversible; potential is given for the anodic and cathodic waves, for oxidation and reductions, respectively.

^cAdsorption on primary electrode surface.

^dFrom Ref. [36].

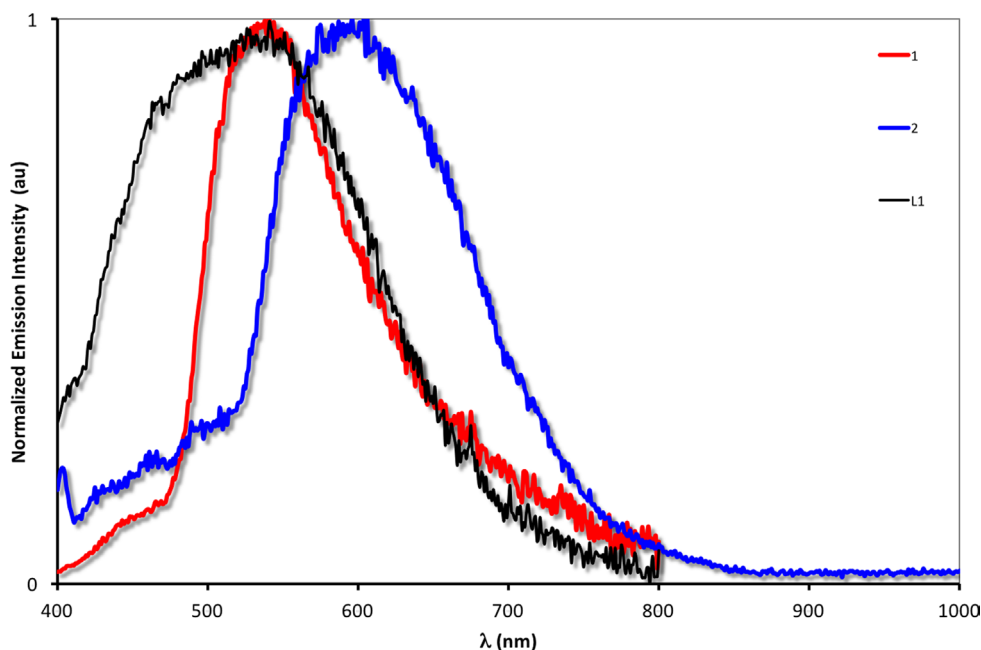


Figure 6. Normalized emission spectra of **L1**, **1**, and **2** at room temperature in degassed acetonitrile ($\lambda_{\text{exc}} = 360$ nm).

quasi-reversible and one irreversible ligand-based reduction waves, assigned by DFT, are observed for **2**. For this complex, the irreversible peak at -2.11 V is due to adsorption on the primary glassy carbon electrode, and the transfer of electrons associated with these peaks could not be determined unambiguously. As expected, due to the anionic nature of **L1** in **2**, the oxidation and reduction potentials of **2** are more cathodically shifted compared to those of **1**. The higher energy calculated for the HOMO of **2** ($E_{\text{HOMO}} = -5.26$ eV) compared with those of $[\text{Ir}(\text{ppy})_2(\text{bpy})]^+$ ($E_{\text{HOMO}} = -5.54$ eV) and **1** ($E_{\text{HOMO}} = -5.53$ eV) is in agreement with the lower oxidation potential of **1** compared to that of $[\text{Ir}(\text{ppy})_2(\text{bpy})]^+$ and **2**, thus confirming the enhanced electron-richness found in **2**, relative to the behavior of $[\text{Ir}(\text{ppy})_2(\text{bpy})]^+$ and **1**.

3.5. Emission properties of **1** and **2**

The emission spectra of **1** and **2** in degassed MeCN at room temperature are shown in figure 6. Upon excitation at 360 nm, **L1**, **1**, and **2** were all found to be poorly emissive with emission maxima, λ_{em} , at 540, 541, and 590 nm, respectively. Similar to $[\text{Ir}(\text{ppy})_2(\text{bpy})]\text{PF}_6$ [36], the emission spectra for **1** and **2** are broad and featureless, indicative of mixed ^3CT emission. The CT emissions are the result of mixed LLCT and MLCT transitions that is mostly LLCT in nature and involves the pyridine moieties of **L1** and **aL1** (where **aL1** = 3-(pyridin-2-yl)benzo[e][1,2,4]thiadiazin-2-ide-1-oxide) in **1** and **2**, respectively. Both complexes exhibited two-component emission decay kinetics and the associated lifetimes (τ_e)

Table 7. Solution state emission data^a of **L1**, **1**, **2** and $[\text{Ir}(\text{ppy})_2(\text{bpy})]\text{PF}_6$ in acetonitrile at room temperature.

Compound	λ_{em} (nm)	τ_e (ns)	Φ_{PL} (%)
L1	540	–	–
1	541	5.3 (4.4%), 395.3 (95.6%)	1.1
2	590	47.8 (47.5%), 129.3 (52.5%)	2.5
$[\text{Ir}(\text{ppy})_2(\text{bpy})]\text{PF}_6^{\text{b}}$	602	275	9.3

^aUsing quinine sulfate as quantum yield standard ($\lambda_{\text{em}} = 450$ nm in MeCN, $\Phi_f = 54.6\%$ in 0.5 M H_2SO_4 as found in Ref. [16]).

^bFrom Ref. [36].

are summarized in table 7. The major decay components of both the complexes fall in submicrosecond regime, similar to that of $[\text{Ir}(\text{ppy})_2(\text{bpy})]\text{PF}_6$ [36], indicating phosphorescence emission profiles. The photoluminescence quantum yields, Φ_{PL} , of **1** and **2** were very low at 1.1 and 2.5%, respectively. Consistent with the electrochemical data, the emission maximum of **1** was blue-shifted by 61 nm (1873 cm^{-1}) relative to that of $[\text{Ir}(\text{ppy})_2(\text{bpy})]\text{PF}_6$ ($\lambda_{\text{em}} = 602\text{ nm}$). This trend in emission is consistent with that observed in absorption where the $^1\text{MLCT}$ maximum of **1** is also blue-shifted by $\sim 50\text{ nm}$ (2708 cm^{-1}) with respect to that of $[\text{Ir}(\text{ppy})_2(\text{bpy})]\text{PF}_6$ (table 3). Concomitant to the larger predicted HOMO–LUMO gap of **2** compared to that of $[\text{Ir}(\text{ppy})_2(\text{bpy})]\text{PF}_6$ (figure 5), and the absorption profiles of **2** and $[\text{Ir}(\text{ppy})_2(\text{bpy})]\text{PF}_6$ ($\Delta\lambda_{\text{abs}(\text{lowest energy})} = 21\text{ nm}$, 1017.15 cm^{-1}), the emission maximum of $[\text{Ir}(\text{ppy})_2(\text{bpy})]\text{PF}_6$ was red-shifted compared to that of **2** ($\Delta\lambda_{\text{em}} = 12\text{ nm}$, 338 cm^{-1}). The trends in emission maxima of **1** and **2** differ unusually from the trends in their respective HOMO–LUMO gaps, calculated by singlet TD-DFT, which indicates that the triplet excited state of **2** is more stabilized compared to that of **1**.

4. Conclusion

Two new Ir(III) complexes, **1** and **2**, bearing the unusual ancillary ligand, 3-(pyridin-2-yl)-4*H*-benzo[*e*] [1,2,4]thiadiazine **L1**, have been synthesized and characterized by various analytical techniques. **L1** coordinates to Ir(III) as both neutral and anionic forms depending on the reaction conditions used. In the solid-state structures of these complexes, the fused phenylene ring of **L1** was spatially away from the ppy moiety to overcome steric hindrance. In **2**, **L1** underwent oxidation to the *S*-oxide analog. Both complexes exhibit mixed ligand-centered and charge-transfer transitions at energies lower than 300 nm, with the absorption in **1** trailing further into the visible region. The complexes exhibit facile oxidation of both the metal and the cyclometalating ligand centers and reduction of the ancillary ligand. Both complexes were poorly emissive with the emission of **1** blue-shifted compared to that of **2**.

Supplementary material

CCDC 1445661 and 1445662 contain the supplementary crystallographic data for $[\text{C}_{34}\text{H}_{25}\text{N}_5\text{Ir}] [\text{PF}_6]$ (**1**) and $[\text{C}_{34}\text{H}_{24}\text{N}_5\text{OSIr}]\cdot\text{CH}_2\text{Cl}_2$ (**2**). These data can be obtained free of charge via <http://www.ccdc.cam.ac.uk/conts/retrieving.html>, or from the Cambridge Crystallographic Data Center, 12 Union Road, Cambridge CB2 1EZ, UK; Fax: (+44) 1223–336-033; or E-mail: deposit@ccdc.cam.ac.uk. The research data supporting this publication can be accessed at <http://dx.doi.org/10.17630/f6bed3a1-bc10-464a-83fa-5fa6ac8a9c4b>.

Acknowledgements

EZ-C acknowledges the University of St Andrews for financial support. We thank Umicore AG for the gift of materials. We acknowledge Ms Weiwei Zheng for initial synthetic efforts. We thank the EPSRC UK National Mass Spectrometry Facility at Swansea University for analytical services. We are grateful to the EPSRC for financial support from grant EP/M02105X/1. JMR would like to thank NSERC Canada, the Canada Research Chair Program and CFI/ORF for financial support. KP acknowledges financial support through the Ontario Trillium Scholarship program.

Disclosure statement

No potential conflict of interest was reported by the authors.

Funding

This work was supported by the Engineering and Physical Sciences Research Council (EPSRC) [grant number EP/M02105X/1].

ORCID

David B. Cordes  <http://orcid.org/0000-0002-5366-9168>

Eli Zysman-Colman  <http://orcid.org/0000-0001-7183-6022>

References

- [1] K.A. King, R.J. Watts. *J. Am. Chem. Soc.*, **109**, 1589 (1987).
- [2] C. Ulbricht, B. Beyer, C. Friebe, A. Winter, U.S. Schubert. *Adv. Mater.*, **21**, 4418 (2009).
- [3] R.D. Costa, E. Ortí, H.J. Bolink, F. Monti, G. Accorsi, N. Armadori. *Angew. Chem. Int. Ed.*, **51**, 8178 (2012).
- [4] S. Sato, T. Morikawa, T. Kajino, O. Ishitani. *Angew. Chem. Int. Ed.*, **52**, 988 (2013).
- [5] B. Wang, Y. Liang, H. Dong, T. Tan, B. Zhan, J. Cheng, K.K.-W. Lo, Y.W. Lam, S.H. Cheng. *ChemBioChem.*, **13**, 2729 (2012).
- [6] J.-B. Kim, S.-H. Han, K. Yang, S.-K. Kwon, J.-J. Kim, Y.-H. Kim. *Chem. Commun.*, **51**, 58 (2015).
- [7] N.M. Shavaleev, G. Xie, S. Varghese, D.B. Cordes, A.M.Z. Slawin, C. Momblona, E. Ortí, H.J. Bolink, I.D.W. Samuel, E. Zysman-Colman. *Inorg. Chem.*, **54**, 5907 (2015).
- [8] J. Zienkiewicz, A. Fryszkowska, K. Zienkiewicz, F. Guo, P. Kaszynski, A. Januszko, D. Jones. *J. Org. Chem.*, **72**, 3510 (2007).
- [9] J. Zienkiewicz, P. Kaszynski, V.G. Young Jr. *J. Org. Chem.*, **69**, 7525 (2004).
- [10] E.R. Clark, J.J. Hayward, B.J. Leontowicz, D.J. Eisler, J.M. Rawson. *Cryst. Eng. Comm.*, **16**, 1755 (2014).
- [11] E.R. Clark, M.U. Anwar, B.J. Leontowicz, Y. Beldjoudi, J.J. Hayward, W.T.K. Chan, E.L. Gavey, M. Pilkington, E. Zysman-Colman, J.M. Rawson. *Dalton Trans.*, **43**, 12996 (2014).
- [12] M. Nonoyama. *Bull. Chem. Soc. Jpn.*, **47**, 767 (1974).
- [13] V.V. Pavlishchuk, A.W. Addison. *Inorg. Chim. Acta*, **298**, 97 (2000).
- [14] G.A. Crosby, J.N. Demas. *J. Phys. Chem.*, **75**, 991 (1971).
- [15] S. Fery-Forgues, D. Lavabre. *J. Chem. Educ.*, **76**, 1260 (1999).
- [16] W.H. Melhuish. *J. Phys. Chem.*, **65**, 229 (1961).
- [17] *CrystalClear-SM Expert v2.0 and v2.1*. Rigaku Americas/Rigaku Corporation, The Woodlands, Texas, USA/Tokyo, Japan (2010–2013).
- [18] P.T. Beurskens, G. Beurskens, R. de Gelder, S. Garcia-Granda, R.O. Gould, R. Israel, J.M.M. Smits. *DIRDIF-99*, Crystallography Laboratory, University of Nijmegen, The Netherlands (1999).
- [19] G.M. Sheldrick. *Acta Crystallogr., Sect. C*, **71**, 3 (2015).
- [20] *CrystalStructure v4.1*. Rigaku Americas/Rigaku Corporation, The Woodlands, Texas, USA/Tokyo, Japan (2013).
- [21] M.J. Frisch, G.W. Trucks, H.B. Schlegel, G.E. Scuseria, M.A. Robb, J.R. Cheeseman, J.A. Montgomery, T.J. Vreven, K.N. Kudin, J.C. Burant, J.M.S. Millam, J. Tomasi, V. Barone, B. Mennucci, M. Cossi, G. Scalmani, N. Rega, G.A. Petersson, H. Nakatsuji, M. Hada, M. Ehara, K. Toyota, R. Fukuda, J. Hasegawa, M. Ishida, T. Nakajima, Y. Honda, O. Kitao, H. Nakai, M. Klene, X. Li, J.E. Knox, H.P. Hratchian, J.B. Cross, C. Adamo, J. Jaramillo, R. Gomperts, R.E. Startmann, O. Yazyev, A.J. Austin, R. Cammi, C. Pomelli, J.W. Ochterski, P.Y. Ayala, K. Morokuma, G.A. Voth, P. Salvador, J.J. Dannenberg, V.G. Zakrzewski, J.M. Dapprich, A.D. Daniels, M.C. Strain, O. Farkas, D.K. Malick, A.D. Rabuck, K. Raghavachari, J.B. Foresman, J.V. Ortiz, Q. Cui, A.G. Baboul, S. Clifford, J.B. Cioslowski, G. Liu, A. Liashenko, I. Piskorz, L.M.R. Komaromi, D.J. Fox, T. Keith, M.A. Al-Laham, C.Y. Peng, A. Manayakkara, M. Challacombe, P.M.W. Gill, B.G. Johnson, W. Chen, M.W. Wong, C. Gonzalez, J.A. Pople, *Gaussian 2003, Revision C.02*, Gaussian Inc., Pittsburgh (2003).
- [22] A.D. Becke. *J. Chem. Phys.*, **98**, 5648 (1993).
- [23] C. Lee, W. Yang, R.G. Parr. *Phys. Rev. B: Condens. Matter*, **37**, 785 (1988).
- [24] A.D. McLean, G.S. Chandler. *J. Chem. Phys.*, **72**, 5639 (1980).
- [25] P.J. Hay, W.R. Wadt. *J. Chem. Phys.*, **82**, 270 (1985).
- [26] M.E. Casida, C. Jamorski, K.C. Casida, D.R. Salahub. *J. Chem. Phys.*, **108**, 4439 (1998).
- [27] R.E. Stratmann, G.E. Scuseria, M.J. Frisch. *J. Chem. Phys.*, **109**, 8218 (1998).
- [28] M. Cossi, N. Rega, G. Scalmani, V. Barone. *J. Comput. Chem.*, **24**, 669 (2003).
- [29] M. Cossi, V. Barone. *J. Chem. Phys.*, **115**, 4708 (2001).
- [30] V. Barone, M. Cossi. *J. Phys. Chem. A*, **102**, 1995 (1998).
- [31] N.M. O'boyle, A.L. Tenderholt, K.M. Langner. *J. Comput. Chem.*, **29**, 839 (2008).
- [32] L. Skripnikov. *Chemissian v4.38*, 2015, copyright 2005–2015. Available online at <http://www.chemissian.com>.
- [33] D.A. Zhurko, G.A. Zhurko. *ChemCraft 1.5*, Plimus, San Diego, CA. Available online at <http://www.chemcraftprog.com>.
- [34] E.R. Clark, J.J. Hayward, B.J. Leontowicz, M.U. Anwar, M. Pilkington, J.M. Rawson. *Dalton Trans.*, **44**, 2071 (2015).
- [35] K.K.-W. Lo, J.S.-W. Chan, L.-H. Lui, C.-K. Chung. *Organometallics*, **23**, 3108 (2004).
- [36] S. Ladouceur, D. Fortin, E. Zysman-Colman. *Inorg. Chem.*, **50**, 11514 (2011).